Determination of optimal residual stress profiles for improved rolling contact fatigue resistance

Hamidreza Mahdavi [1,*], *Konstantinos* Poulios [1] , and *Christian F.* Niordson [1]

[1]Department of Mechanical Engineering, Section of Solid Mechanics, Technical University of Denmark, Nils Koppels Allé, Building 404, DK-2800 Kgs. Lyngby

Abstract. A theoretical framework is developed for the evaluation of favorable residual stress profiles, suppressing fatigue damage initiation in rolling contact fatigue. Non-metallic inclusions at the microstructure of bearings are one of the most important reasons for fatigue damage initiation since they act as stress risers. In order to evaluate the stress state around such inclusions at the micro-scale, macroscopic stress histories are determined by Hertzian contact theory at different depths below the raceway for a typical roller bearing. These stress distributions are then used as far-field stresses for a micro-scale model accounting for single inclusions of different geometries and orientations. Eshelby's method is used to relate far-field and local stresses in the vicinity of inclusions. The von Mises stress criterion is then used as a conservative estimator of crack initiation due to micro-scale plasticity. The effect of compressive residual stresses added to the axial and circumferential normal stress components at different depths is analyzed. The von Mises stress field around different inclusions at different depths is investigated in order to determine the most critical case in terms of micro-scale plastic deformation. Finally, an optimization process is carried out in order to determine the residual stresses that minimize the maximum observed von Mises stress as a function of depth.

Keywords: Rolling contact fatigue; Non-metallic inclusions; Residual stresses; Fatigue damage initiation

1 Introduction

Rolling element bearings are widely used in modern machinery like wind turbines, aerospace applications, engines, etc. to support rotary elements. Surface originated pitting and subsurface initiated spalling are the most relevant bearing failure mechanisms [1, 2]. While, surface initiated pitting can be mainly observed under poor lubrication conditions [3], well-lubricated bearings with smooth contact surfaces typically fail due to subsurface initiated rolling contact fatigue with cracks initiating at non-metallic inclusions [1, 4].

Accurate life time prediction for bearings is still a very important topic of research. In this context, the concept of a material fatigue limit, defined as a stress below which no

* Corresponding author: hamah@mek.dtu.dk

material deterioration is expected, is acknowledged by the industry [5]. Many researchers have included the material fatigue limit concept in their service life estimations for bearings, such as Ioannides and Harris [6, 7]. Using Eshelby's method to study the effect of inclusions on the endurance limit of bearing steels is a further method employed by researchers such as Courbon et al. [8] and Lamagnere et al. [9]. Lai et al. [10], developed a deterministic defect model to describe the fatigue crack growth from debonded hard inclusions and then combined it with a stochastic model that describes the inclusion size distribution to predict the fatigue limit of bearing steels. Later, they also validated their results by conducting an experimental study [11]. More recently, Allison and Pandkar [12] employed a 2D finite element model to investigate the critical factors that affect the fatigue limit of bearing steels accounting among other for inclusion geometry and temperature dependent mechanical properties.

As mentioned above, crack initiation can be related to micro-scale plasticity due to stress concentrations around non-metallic inclusions. Adding compressive residual stresses to offset the stress state, can therefore delay crack initiation by suppressing micro-scale localized plasticity. The majority of available studies supports the beneficial effect of compressive residual stresses on the fatigue life of bearings [13, 14, 15, 16]. In general, heat treatments and plastic deformation, e.g. during running-in of a bearing, are the most relevant sources of compressive residual stresses [17]. Voskamp and Mittemeijer [18] concluded that applying a general state of compressive residual stresses improves the fatigue life of bearings through suppressing the possibility of yielding. Popinceanu et al. [19] compared different hypotheses regarding the critical stresses in rolling contact fatigue and concluded that von Mises stress is appropriate for evaluating the effect of residual stresses on fatigue life as it takes into account all components of the stress field. Bhargava, et al. [20], Bower and Johnson [21], and Howell, et al. [22] were among the first researchers who developed finite element models for rolling contact taking the effect of residual stresses into account. Warhadpande et al. [23] developed a 2D plane-strain J2 based plasticity model including linear and non-linear kinematic hardening laws to investigate the influence of plasticity-induced residual stresses on rolling contact fatigue. Shen et al. [24] developed a two dimensional finite element model based on continuum damage mechanics to investigate the effects of retained austenite and residual stresses on rolling contact fatigue and compared their results with experiments. Walvekar and Sadeghi [25] developed an elastoplastic finite element model based on micro-indentation tests and investigated the effect of residual stresses induced due to carburization process. A similar research on refurbished case carburized bearings was conducted in [26]. Guan et al. [27] developed a continuum damage mechanics based model to evaluate the damage evolution of M50 bearing steel considering residual stresses induced by shot peening. Ooi et al. [28] investigated the effect of retained austenite and residual stress on rolling contact fatigue of carburized steel numerically based on a 2D extended finite element model and experimentally. Golmohammadi et al. [29] developed a 3D elastoplastic finite element model to characterize the rolling contact fatigue behavior of through hardened steel at high loads incorporating compressive residual stresses induced by plastic deformation.

In this study, a semi-analytical method is proposed based on the von Mises criterion for studying the effect of superimposed compressive stresses on subsurface crack initiation in rolling contact fatigue. A plane-strain finite element model is used to determine macroscopic stress histories at different depths below a Hertzian contact. The stress distributions obtained are then applied as far-field stresses for a 3D micro-scale model accounting for inclusions of different geometries and orientations. Far-field stresses and local stresses around inclusions are linked using Eshelby's method. Using von Mises stress as an indicator for crack initiation due to micro-scale plasticity, optimal compressive residual stresses added to the axial and circumferential stress components are determined as a function of depth.

2 Analytical procedures

In the first part of this section, the analytical method employed for studying the effect of residual stresses is described. A method for obtaining optimal initial residual stresses as a function of the depth into the material is then presented in the second part.

2.1 Analytical model

In a typical roller bearing, assuming a frictionless line contact between a roller and a raceway, Hertzian contact theory can be used to determine subsurface stress histories at different depths y below the raceway for any arbitrary Hertzian pressure σ_H. Such stresses, obtained based on the assumption of a homogenous material, will be referred to as macroscopic stresses. For a periodic load, these are the stress histories a material point below the surface will experience during every loading cycle. In the present study, macroscopic stress histories at different depths are obtained through a 2D plane-strain finite element model. The 3D stress state histories extracted at each depth are then applied as far-field stresses for a micro-scale model accounting for the presence of non-metallic inclusions (cf. Fig. 1). In the coordinate system shown in Fig. 1, x, y, and z represent the circumferential, radial and axial directions, respectively.
In general, for a fully bonded elastic ellipsoidal inclusion inside an infinite elastic matrix, the local stress field around the inclusion can be found analytically by Eshelby's method [30, 31] much more efficiently than using numerical methods [9]. Hence, Eshelby's method is applied in this study to relate the far-field macroscopic stresses to local stresses around non-metallic inclusions. In particular, among the different available implementations of Eshelby's method, results presented in this paper are based on the code by Meng et al. [32].

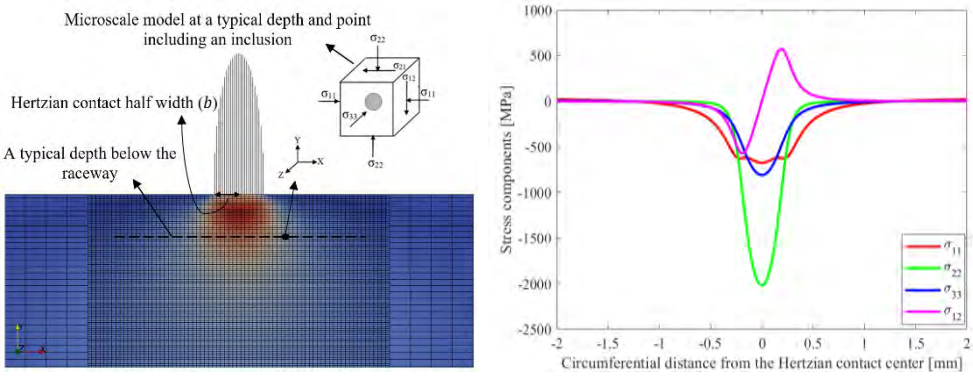

(a) (b)

Fig. 1. Determination of macroscopic stress histories: (a) Schematic view of the 2D plane-strain finite element model, (b) Stress components at a typical depth below the surface ($y = -0.54\ b$).

Let σ_{kl} be a macroscopic far-field stress tensor that is in general a function of loading history and depth y. Then, assuming an ellipsoidal inclusion at a specific depth, the idea is to find the corresponding stress field $\tilde{\sigma}_{ij}$ around the inclusion at the microscale using Eshelby's method. The microscale stress will depend on the location around the inclusion but also on the time and the depth that the assumed inclusion is considered at (cf. Fig. 1a). To relate the components of the far-field stress state σ_{kl} to the microscopic one $\tilde{\sigma}_{ij}$ at each specific point around the inclusion, a stress concentration tensor T_{ijkl} can be defined, such that

$$\tilde{\sigma}_{ij} = T_{ijkl}\sigma_{kl} \tag{1}$$

Since the problem is linear, T_{ijkl} is independent of time t and the distance y between the inclusion and the surface, and it will only depend on the shape of the inclusion and the considered location around it. By applying a unit far-field stress for each component of σ_{kl} in Eshelby's method, the local stress tensor obtained will determine the corresponding components of the stress concentration tensor based on Eq. (1). Repeating this procedure for all six components of σ_{kl} yields the whole stress concentration tensor T_{ijkl}. By determining once at the beginning a set of tensors T_{ijkl} for multiple points around the inclusion, these can subsequently be used in Eq. (1) throughout the whole time history as well as for investigating the behavior of the same type of inclusion at different depths.

2.2 Determination of an optimal residual stress

Of course, if residual stresses are present at the macroscopic scale, the stress history $\sigma_{kl}(t)$ at each specific depth has to be modified accordingly. In components with superimposed residual stresses due to heat treatment, the radial component of these stresses is practically negligible, while the circumferential and axial components are of similar magnitude. Hence, one possible scenario of superimposed compressive residual stresses σ_{res} at the macroscale can be represented by the following shift in stress space

$$\hat{\sigma}_{kl}(t, \sigma_{res}) = \sigma_{kl}(t) + \begin{bmatrix} -\sigma_{res} & 0 & 0 \\ 0 & 0 & 0 \\ 0 & 0 & -\sigma_{res} \end{bmatrix}. \tag{2}$$

One can then calculate von Mises stresses $\sigma_{VM}(t)$ and $\hat{\sigma}_{VM}(t, \sigma_{res})$, respectively based on the unmodified stress history σ_{kl} or the modified stress history $\hat{\sigma}_{kl}$ with the superimposed residual stress. Fig. 2 shows the effect of an arbitrary added residual stress on the two affected stress components and the von Mises stress at the macroscale. It is evident that the significant reduction in the maximum attained von Mises stress can be seen as a means for suppressing or delaying the onset of plasticity.

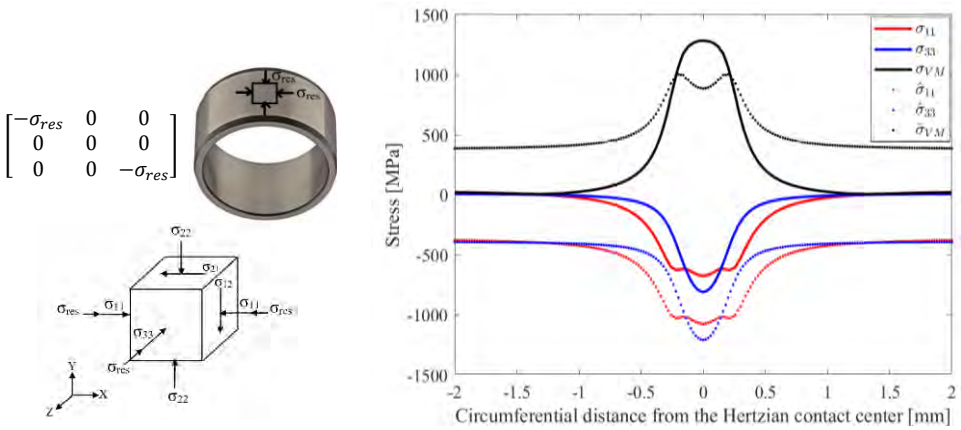

Fig. 2. Effect of a residual stress of $-0.17\sigma_H$ on the von Mises stresses at $y = -0.54\ b$.

For realistic bearing loads, macroscale plasticity is not a real concern, but the same concept can also be applied to the microscale, where microscale plasticity close to an inclusion is a common fatigue crack initiation mechanism. To this end, a cloud of points around an inclusion is considered as illustrated conceptually in Fig. 3. Knowing the stress concentration tensor $T_{ijkl}^{<P>}$ for any point P in the cloud, the local stress tensor can be obtained by Eq. (1), including the effect of residual stresses from Eq. (2), leading finally to von Mises stresses as

$$\sigma_{VM}^{<P>}(t,\sigma_{res}) = \sqrt{\frac{(\hat{\sigma}_{11}-\hat{\sigma}_{22})^2+(\hat{\sigma}_{22}-\hat{\sigma}_{33})^2+(\hat{\sigma}_{33}-\hat{\sigma}_{11})^2+6\hat{\sigma}_{12}^2}{2}} \text{ with } \hat{\sigma}_{ij} = T_{ijkl}^{<P>}\hat{\sigma}_{kl}. \quad (3)$$

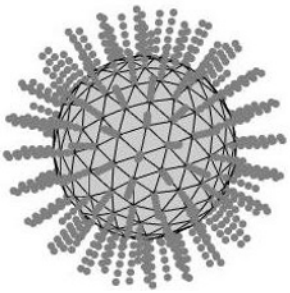

Fig. 3. Cloud of points around a spherical inclusion.

It should be noted that the superimposed residual stresses have both deviatoric and hydrostatic contributions. Nevertheless, by employing Eq. (1), the von Mises stresses at the microscale will in general not only depend on the deviatoric macroscopic stresses but also on the hydrostatic ones.

Based on the assumption that crack nucleation occurs due to microscale cyclic plasticity close to an inclusion, the maximum von Mises stress obtained in an elastic calculation during a complete loading cycle can be used as an indicator of crack nucleation. The idea now is to determine an optimal value σ_{res}^{*} of the compressive residual stress σ_{res} that will minimize the maximum local von Mises stress throughout a loading cycle and among all points around the inclusion:

$$\sigma_{res}^{*} \leftarrow \min_{\sigma_{res}} \max_{t} \max_{P} \sigma_{VM}^{<P>}(t,\sigma_{res}). \quad (4)$$

This univariate minimization problem could be solved using any available single variable minimizer, but for simply demonstrating the concept, a brute force approach is also sufficient. In the present work a range of values is simply swept for σ_{res} with fixed increments. For any probed residual stress value, the time step and point around the inclusion are determined, which correspond to the maximum von Mises stress, according to the inner two max operators in Eq. (4). Then, the optimum σ_{res}^{*} value is determined by comparing the obtained maximum von Mises among all probed σ_{res} values. It should be mentioned that the process has to be repeated at different depths y from the surface, ultimately leading to an optimal residual stresses profile $\sigma_{res}^{*}(y)$, as a function of depth, y.

3 Results and discussion

In this section, geometrical and material parameters used in this study are provided first, followed by von Mises stresses calculated without and with inclusions, and finally, the effect of superimposed compressive residual stresses is investigated.

3.1 Geometrical and material information

An 81212 thrust bearing with the geometrical and mechanical properties summarized in Table 1 forms the basis for this study. A spherical aluminium oxide inclusion with a diameter of 5μm is considered, as well as corresponding prolate ellipsoidal inclusions with an aspect ratio of 3. Young's modulus and Poisson's ratio of aluminium oxide are chosen as 375 GPa and 0.25 while the respective values for the steel matrix are 203 GPa and 0.3, [12].

Table 1. Thrust bearing geometrical and material parameters used in this study.

Inner diameter	Outer diameter	Number of rollers	Roller element length	Hertzian pressure (σ_H)	Hertzian contact half width (b)
60 mm	95 mm	20	10.5 mm	2.3 GPa	0.22 mm

3.2 Von Mises stresses without superimposed compressive stresses

Microscale von Mises stresses are calculated at a large number of points around the inclusion analyzed at 16 different depths from the surface. Table 2 summarizes the maximum von Mises stresses attained for a spherical inclusion as well as for ellipsoidal inclusions at different orientations. Some selected cases are illustrated in more detail in Fig. 4. Compared to the macroscale maximum von Mises stress, the presence of a spherical inclusion leads to a maximum microscale von Mises stress increased by a factor of 1.31. For the ellipsoidal inclusion, the corresponding stress concentration factor varies from 1.29 to 1.55 for the different directions, with the maximum attained for the 90° orientation of the major axis with respect to the circumferential direction.

Table 2. Maximum von Mises stress for the spherical and different ellipsoidal inclusions.

	Without inclusion	Spherical	Ellipsoidal				
			0º	30º	45º	60º	90º
Maximum von Mises stress (MPa)	1308	1719.3	1691.4	1713.2	1844.6	1946.3	2029.5
Concentration factor	1	~1.31	~1.29	~1.31	~1.41	~1.49	~1.55

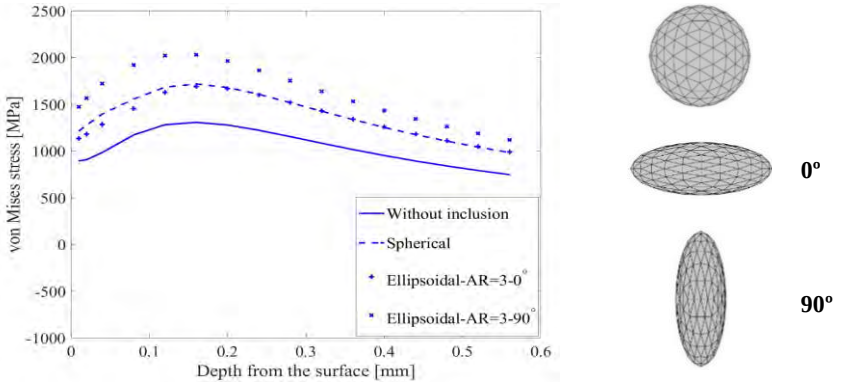

Fig. 4 Von Mises stresses as a function of depth.

3.3 Optimal residual stress profiles

The effect of superimposed compressive stresses is investigated for the most critical case, which is the ellipsoidal inclusion with its major axis in radial direction. For this purpose, σ_{res} is varied from -800 MPa to 0 MPa in fixed increments of 5 MPa. Fig. 5 depicts the original microscale von Mises stresses and the optimized ones, after adding the optimal residual stress profile $\sigma^*_{res}(y)$, obtained according to section 2.2. The latter is also plotted in the diagram. A significant reduction of the maximum von Mises stresses throughout the investigated depths can be observed in the figure. Presuming a relationship between the onset of microscale plasticity and fatigue crack initiation, a reduced probability of fatigue damage can also be anticipated. In addition, after superimposing the favorable compressive residual stresses profile, the depth of maximum von Mises stress shifts from 0.16 mm to 0.12 mm.

Figure 6 shows the critical points around the inclusion, where the von Mises stress attains its maximum value before and after the superposition of macroscopic residual stresses. Without residual stresses, microscale plasticity is expected to occur at the top and bottom of the ellipsoidal inclusion, with respect to the radial direction. However, the addition of residual stresses shifts the location of the critical points to the equator of the inclusion. Hence, one could anticipate a change in the location of fatigue damage initiation.
Figure 7 identifies the occurrence of maximum von Mises stress at the microscale during the applied macroscopic stress histories. Before the addition of compressive residual stresses, the maximum von Mises at the microscale occurs when the inclusion is approximately below the Hertzian contact center, while this maximum shifts to the location of maximum orthogonal shear stresses at a lower depth, after the addition of residual stresses. In other words, fatigue damage initiation will probably be governed by the radial component of the macroscale stress in one case and by the macroscale orthogonal shear stress in the other case.

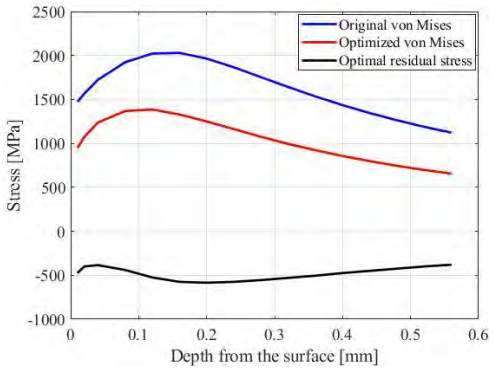

Fig. 5. Optimal residual stress profile along the depth direction and its effect on the maximum von Mises stress for a 90 º ellipsoidal inclusion with AR=3.

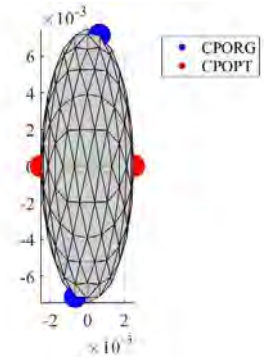

Fig. 6. Critical points around the inclusion without (CPORG) and with (CPOPT) residual stresses.

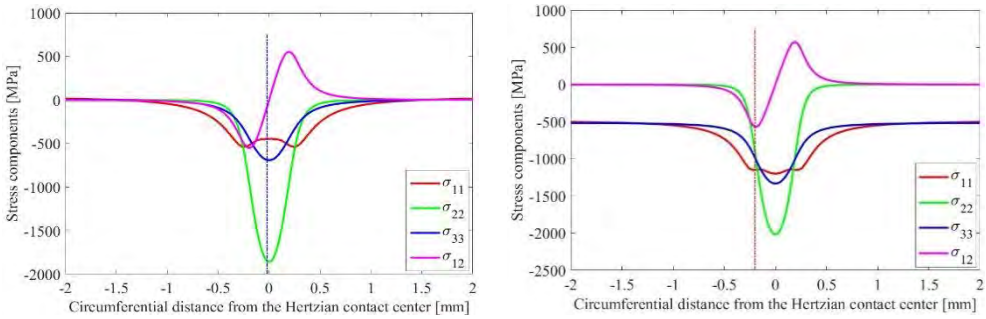

(a) (b)

Fig. 7. Location of the maximum microscopic von Mises stress during the loading history: (a) without residual stresses, (b) with optimal residual stresses.

4 Conclusions

In this study, a theoretical method is proposed for evaluating favorable residual stress profiles, aiming to suppress fatigue damage initiation around non-metallic inclusions in rolling contact fatigue. A study among different inclusions reveals that radially elongated ellipsoidal inclusions lead to the largest stress concentration factor in terms of maximum von Mises stress. For this critical case, employing the proposed method for determining optimal compressive residual stresses has led to a remarkable reduction in the maximum von Mises

stresses and consequently the possibility of fatigue damage initiation. It has also been found that superposition of the obtained residual stresses profile changes the site of fatigue damage initiation around the inclusion. Moreover, either the macroscopic orthogonal shear stress or the macroscopic radial stress component may govern the onset of microscale plasticity depending on whether compressive residual stresses are added or not. Finally, the existence of an optimal level of compressive residual stresses, suggests that excessive compressive residual stresses might lead to no improvement or even deterioration of fatigue properties, as argued e.g. in [33].

Acknowledgements: This work is supported by the Innovation Fund Denmark grant with number 7046-00003B. The authors would also like to thank project collaborator Yuri Kadin from SKF for his valuable input.

References

1. W.E. Littmann. *The mechanism of contact fatigue*. NASA Spec Report, SP-237 n.d.

2. W.E. Littmann, R.L. Widner. Propagation of contact fatigue from surface and subsurface origins. J Basic Eng, **88**: 624-636 (1996)

3. A.F. Bower. The influence of crack face friction and trapped fluid on surface initiated rolling contact fatigue cracks. J Tribol, **110:** 704-711 (1988)

4. T.A. Harris. *Rolling bearing analysis.* Wiley, New York (2001)

5. International Organization for Standards. *Dynamic load ratings and rating life.* ISO: Int Organ Stand (2007)

6. E. loannides, T. A. Harris. A new fatigue life model for rolling bearings. J Tribol, **107:** 367-377 (1985)

7. T. A. Harris. Prediction of ball fatigue life in a ball/v-ring test rig. J Tribol, **119:** 365-370 (1997)

8. J. Courbon, G. Lormand, G. Dudragne, P. Daguier, A. Vincent. Influence of inclusion pairs, clusters and stringers on the lower bound of the endurance limit of bearing steels. Tribol Int, **36:** 921-928 (2003)

9. P. Lamagnere, R. Fougeres, G. Lormand, A. Vincent, D. Girodin, G. Dudragne, F. Vergne. A Physically Based Model for Endurance Limit of Bearing Steels. J Tribol, **120**: 421-426 (1998)

10. J. Lai, T. Lund, K. Rydén, A. Gabelli, I. Strandell. The fatigue limit of bearing steels Part I: A pragmatic approach to predict very high cycle fatigue strength. Int J Fatigue, **37**: 155-168 (2012)

11. A. Gabelli, J. Lai, T. Lund, K. Rydén, I. Strandell, G. E. Morales-Espejel. The fatigue limit of bearing steels – Part II: Characterization for life rating standards. Int J Fatigue, **38**: 169-180 (2012)

12. B. Allison, A. Pandkar. Critical factors for determining a first estimate of fatigue limit of bearing steels under rolling contact fatigue. Int J Fatigue, **117**: 396-406 (2018)

13. R.L. Scott, R.K. Kepple, M.H. Miller. The effect of processing induced near surface residual stress on ball bearing fatigue. *Rolling contact phenomenon*, 301-316, Elsevier, Amsterdam (1962)

14. J.O. Almen. Effect of Residual Stress on Rolling Bodies. *Rolling contact phenomenon,* 400–424, Elsevier, Amsterdam (1962)

15. E.V. Zaretsky, R.J. Parker, W.J. Anderson. A Study of residual stress induced during rolling. J Lubr Technol, **91**: 314-319 (1969)

16. K. Maeda, H. Kashimura, N. Tsushima. Investigation on the fatigue fracture of core in carburized rollers of bearings. Tribol T, **29**: 85-90 (1986)

17. G. Donzella, R. Gerosa, C. Petrogalli, B. Rivolta, G. Silva, M. Beretta. Evaluation of the residual stresses induced by shot peening on some sintered steels. Procedia Engineer, **10**: 3399-3404 (2011)

18. A.P. Voskamp, E.J. Mittemeijer. The effect of the changing microstructure on the fatigue behavior during cycling rolling contact loading. Zeitschrift fur Metallkunde, **88**: 310-319 (1997)

19. N.G. Popinceanu, E. Diaconescu, S. Cretu. Critical stresses in rolling contact fatigue. Wear, **71**: 265-282 (1981)

20. V. Bhargava, G.T. Hahn, C.A. Rubin. An elastic–plastic finite element model of rolling contact, part 1: analysis of single contacts. J Appl Mech, **52**: 67-74 (1985)

21. A.F. Bower, K. L. Johnson. The influence of strain hardening on cumulative plastic deformation in rolling and sliding line contact. J Mech Phys Solids, **37**: 471-493 (1989)

22. M. Howell, G. Hahn, C. Rubin, D. McDowell. Finite element analysis for nonlinear kinematic hardening bearing steel. J Tribol, **117**: 729-736 (1995)

23. A.Warhadpande , F. Sadeghi , R. D. Evans, M. N. Kotzalas. Influence of plasticity-induced residual stresses on rolling contact fatigue. Tribol T, **55**: 422-437 (2012)

24. Y. Shen, S. Mobasher Moghadam, F. Sadeghi, K. Paulson, R.W. Trice. Effect of retained austenite – Compressive residual stresses on rolling contact fatigue life of carburized AISI 8620 steel. Int J Fatigue, **75**: 135-144 (2015)

25. A.A. Walvekar, F. Sadeghi. Rolling contact fatigue of case carburized steels. Int J Fatigue, **95**: 264-281 (2017)

26. N.R. Paulson, Z. Golmohammadi, A. A. Walvekar, F. Sadeghi, K. Mistry. Rolling contact fatigue in refurbished case carburized bearings. Tribol Int, **115**: 348-364 (2017)

27. J. Guan, L. Wang, Y. Mao, X. Shi, X. Ma, B. Hu. A continuum damage mechanics based approach to damage evolution of M50 bearing steel considering residual stress induced by shot peening. Tribol Int, **126**: 218-228 (2018)

28. G.T.C. Ooi, S. Roy, S. Sundararajan. Investigating the effect of retained austenite and residual stress on rolling contact fatigue of carburized steel with XFEM and experimental approaches. Mat Sci Eng A, **732**: 311-319 (2018)

29. Z. Golmohammadi, A. Walvekar, F. Sadeghi. A 3D efficient finite element model to simulate rolling contact fatigue under high loading conditions. Tribol Int, **126**: 258-269 (2018)

30. J.D. Eshelby. Elastic inclusions and inhomogeneities. Prog Solid Mech, **2**: 89-140 (1961)

31. T. Mura, *Micromechanics of defects in solids,* Martinus Nijhoff Publishers, Dordrecht, The Netherlands (1982)

32. C. Meng, W. Heltsley, D.D. Pollard. Evaluation of the Eshelby solution for the ellipsoidal inclusion and heterogeneity. Comput Geosci, **40**: 40-48 (2012)

33. R.K. Kepple, R.L. Mattson. Rolling element fatigue and macroresidual stress. J Lubr Technol, **92**(1): 76-81 (1970)